JOURNAL OF PROPULSION AND POWER
Vol. 20, No. 5, September–October 2004

Maximum Power Tracking and Pulse-Width-Modulated Shunt for Satellite Power Systems

Shengyi Liu,* Roger A. Dougal,† and Eugene V. Solodovnik‡
University South Carolina, Columbia, South Carolina 29208

The feasibility is evaluated of using the continuous maximum power operation to lower the operating temperature and to achieve the highest efficiency for solar cells deployed in space, which are subject to thermally induced efficiency degradations and partial failure of cells due to microextraterrestrial objects' impinging or mechanical stress during deployment. The solar array is constantly operated at its maximum power point through a maximum power point tracker, delivering power to the load, the battery, and the shunt that is controlled by a pulse-width modulator to facilitate the tracker with variable impedance, so that the conditions for a maximum power transfer can always be satisfied regardless of the variation in the array internal resistance. It is shown that the proposed design can achieve the best efficiency and the lowest operating temperature compared to conventional regulation methods. The design also results in minimized bus voltage ripples and increased voltage regulation capabilities.

Nomenclature

A	=	solar array front surface area, m^2
A_n	=	normalized solar array area
c_p	=	solar array specific heat, J/kg · K
D	=	percentage of sunshine time in one orbit
H_{ST}	=	satellite altitude, m
m	=	structured solar array mass, kg
m_a	=	solar array specific mass, kg/m^2
m_n	=	normalized specific mass, kg/m^2
N	=	number of orbits in service lifetime
P_L	=	load power, W
P_{SA}	=	solar array generated power, W
q_{SA}	=	solar array radiation cooling rate, W
q_{SS}, q_{EA}, q_{ES}, q_{SP}	=	heat transfer rate by sunshine, by Earth albedo, by Earthshine, and space background temperature, W
q_{ST}	=	heat transfer rate by satellite internal heat, W
$\dot{q}_{ST}$	=	heat flux due to satellite internal heat, W/m^2
R_{EA}	=	Earth radius, 6.378×10^6 m
S	=	solar irradiance in orbit, W/m^2
S_0	=	solar constant, 1366.1 W/m^2
T	=	solar array temperature, K
T_{EA}	=	Earth equilibrium temperature, K
T_{max}, T_{min}	=	solar array maximum and minimum temperatures during sun-view time, K
T_{SP}	=	deep space temperature, 2.73 K
$\alpha_{b,SA}$, $\alpha_{f,SA}$	=	solar array back and front surface absorptance
$\beta_{b,EA}$, $\beta_{b,SP}$, $\beta_{b,ST}$	=	solar array back surface Earth-viewing, space-viewing, and satellite-viewing factor
$\beta_{f,EA}$, $\beta_{f,SP}$, $\beta_{f,ST}$	=	solar array front surface Earth-viewing, space-viewing, and satellite-viewing factor
Γ	=	satellite orbit period, s
γ	=	radiation degradation factor at end of life
δ	=	solar array power transfer factor
ε_{EA}	=	Earth emittance, ~0.75
$\varepsilon_{b,SA}$, $\varepsilon_{f,SA}$	=	solar array back and front surface emittance
ε_{SP}	=	space emittance, 1.0
η	=	solar array efficiency
ϑ	=	solar array thermal swing time, s
κ_{EA}, κ_{ES}, κ_{ST}	=	coefficient of equivalent sunshine due to Earth albedo, due to Earthshine, and due to internal heat
μ	=	Earth gravitational parameter, 3.994×10^{14} m^3/s^2
ρ_{EA}	=	Earth albedo, ~0.35
$\rho_{f,SA}$, $\rho_{b,SA}$	=	solar array front and back surface reflectance
σ	=	Stephan–Boltzmann constant, 5.67×10^{-8} W/m^2 · K^4
τ_{AT}	=	Earth atmospheric transmittance, ~0.736
Φ	=	unit step function

Received 22 June 2003; presented as Paper 2003-6037 at the 1st International Energy Conversion Engineering Conference, Portsmouth, VA, 17 August 2003; revision received 9 December 2003; accepted for publication 9 December 2003.

*Associate Research Professor, Department of Electrical Engineering; lius@engr.sc.edu. Member AIAA.
†Professor, Department of Electrical Engineering.
‡Assistant Research Professor, Department of Electrical Engineering.

Introduction

IT is well known that the temperature-dependent photovoltaic effect of solar arrays shows degrading efficiency as the operating temperature increases.[1,2] Previous research[3] also shows that the temperature has a dramatic effect on the efficiency of an array with a single cell failure, which results in 50% array efficiency drop above a certain elevated temperature and revival of the normal efficiency at room temperature. Solar cells deployed in space are subject to thermally induced performance degradation as well as radiation degradation and sporadic damage of cells in the arrays upon which microextraterrestrial objects impinge. Thermally induced performance degradations are due to some reversible mechanisms such as increased junction recombination and leakage[1] and some nonrecoverable mechanisms such as thermal stress induced damage and formation of blocking contacts.[4] Solar arrays aboard a low Earth orbit (LEO) satellite are exposed to thermal irradiations from direct sunshine, Earth albedo, Earthshine, and also satellite internal heat generation, which cause the array temperature to rise and the efficiency to degrade.

Figure 1 shows the solar spectral irradiance, and Table 1 shows the solar irradiance distribution in spectral bands in orbits. These data were obtained and derived through the SOLAR2000 empirical solar irradiance model[5,6] and categorized based on the International Standards Organization standard[7] for the time of 8 April 2003, 14:10 h. For typical solar cells deployed in space, such as Si- and GaAs-based cells, the majority of the solar power falls beyond the photovoltaic spectrum that ranges from visible to near

Table 1 Solar irradiance distribution in spectral bands[7]

	Band								
Quantity	X-ray	XUV	EUV	UV	VIS	IR	Far IR	Radio	Total
λ, nm	<10	10-30	30-120	120-400	400-700	700-10^4	10^4-10^6	>10^6	
Irradiance, W/m^2	$9.04 \cdot 10^{-4}$	$1.20 \cdot 10^{-3}$	$3.54 \cdot 10^{-3}$	104.8	529.2	731.1	0.974	$6.08 \cdot 10^{-5}$	1366.1
%	$6.62 \cdot 10^{-5}$	$8.79 \cdot 10^{-5}$	$2.59 \cdot 10^{-4}$	7.70	38.7	53.5	$7.13 \cdot 10^{-2}$	$4.45 \cdot 10^{-6}$	100

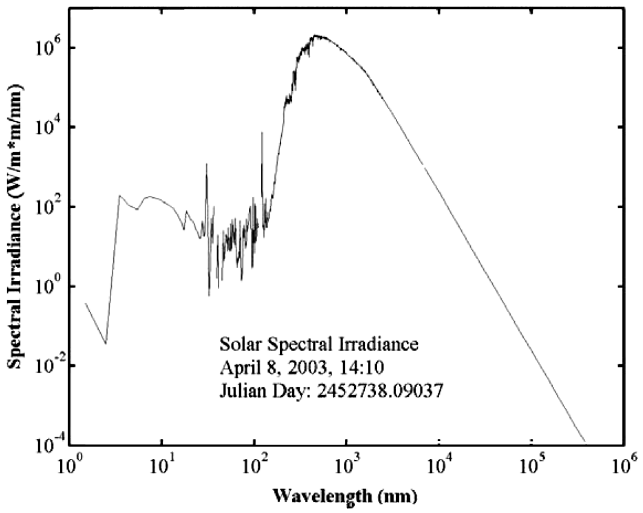

Fig. 1 Solar spectral irradiance in a near Earth orbit on 8 April 2003, 14:10 h (Refs. 5 and 6).

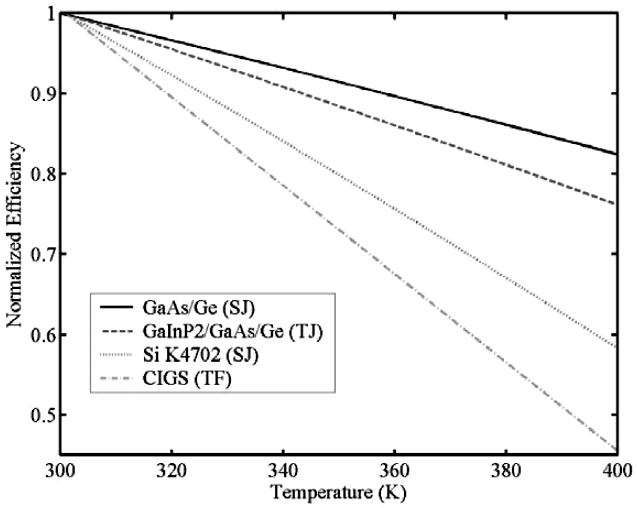

Fig. 2 Normalized efficiencies as functions of temperatures (Ref. 9 and Spectrolab web site).

infrared (IR). When it is considered that the efficiency of the state-of-the-art solar cells is less than 30% (Ref. 8), the percentage of the solar power converted to heat (either due to direct absorption of the energy beyond the photovoltaic spectrum or due to the heat generation from the photovoltaic process) in the cell is >60%. (Data available online, "Spectrolab Photovoltaic Data Sheets: k4702.pdf, sj.pdf, tnj.pdf, and panels.pdf," at URL:http://www.spectrolab.com [cited 20 April 2003].) This conclusion is based on the assumptions that the transmitted energy is generally a very small fraction and that the reflectance is minimal. Whereas the former premise is true of all cells deployed in space, the latter varies and is dependent on cell types and surface coatings. For example, for the GaAs-based triple-junction cell used in the following analysis, the solar absorptance is 0.92, giving a reflectance of 0.08. For the Si single-junction cell, the solar absorptance is 0.74, yielding a much higher reflectance of 0.26. However, because the efficiency of the Si single-junction cell is considerably lower than that of the GaAs-based triple-junction cell, its percentage of solar power converted to heat is still about 60%.

The efficiency losses due to temperature increase for some typical solar cells are graphed in Fig. 2. Here, the efficiency at the beginning of life is used for each cell, and only the reversible thermal degradation mechanisms are included in the analysis. The data for the Si K4702 single-junction cell, the GaAs/Ge single-junction cell, and the GaInP2/GaAs/Ge triple-junction cell are obtained from the SpectroLab website. The $CuIn_{1-x}$ $GaSe_2$ (CIGS) thin-film cell, being lightweight, radiation hard, and currently under development for future space applications,[9,10] is also included in Fig. 2 for comparison. The efficiency for each type of cell is normalized to its value at 301 K (28°C). As illustrated, at 363 K, the efficiency losses for the GaAs-based single-junction cell and triple-junction cell, the Si single-junction cell, and the CIGS thin-film cell are 11, 15, 26, and 34%, respectively. These data show that the performance of solar arrays is significantly degraded if heat is not effectively removed.

One approach to controlling the heat absorption of solar arrays in orbit is to use selective coating that blocks heat irradiation while transmitting the photovoltaic spectrum. However, a coating effectively performing the functions of the heat rejection and the spectrum transmission is difficult to develop. Also a coating developed for one type of cells may not perform well for another type. In addition, the low heat absorptance of coatings also inhibits radiation cooling of the array due to the corresponding low emittance, according to Kirchhoff's law. The purpose of this paper is to investigate the possibility of reducing the temperature of the solar array, thereby increasing its efficiency in terms of system design and operation. When operated at its maximum power point (MPP) constantly, the solar array delivers the maximum possible electrical power to the bus while the power that turns to heat in the cells is minimized. Thus, if operated at the MPP, the solar array undergoes the best cooling effect for given thermal environmental conditions. This is particularly beneficial when a partial failure of cells in an array occurs because the MPP tracking can hold the array at its highest possible power output even if the internal resistance is changed. We propose here a pulse-width-modulation- (PWM-) controlled shunt, the goal of which is to provide a bypass for the excess energy of solar arrays and to facilitate the maximum power extraction. The feasibility of using continuous maximum power operation to reduce the cell operating temperature and, hence, the thermally induced efficiency degradation is evaluated for several solar cells deployed in space. It is shown that the proposed design allows the best efficiency and the lowest operating temperature, thereby having potential benefits for the solar array size and mass reduction and the lifetime enhancement. The design also results in minimized bus voltage ripples and, therefore, minimized size of filters. The description of the proposed fundamental system configuration follows.

System Descriptions

Shown in Figs. 3–5 are three different bus voltage regulation configurations for satellite power systems. Common to all of these configurations is a secondary side across the bus rail, including a filter, a battery array with a charge controller, and a load. All three systems use multipanel solar arrays for power generation, which is practically important to the reliability, transportation, and deployability of solar arrays in orbit. The differences among these configurations include the ways of feeding the array power to the bus and the methods of regulating the bus voltages.

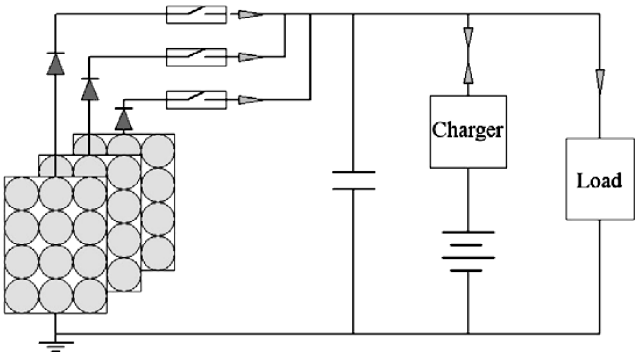

Fig. 3 Sequential series-switching regulation.

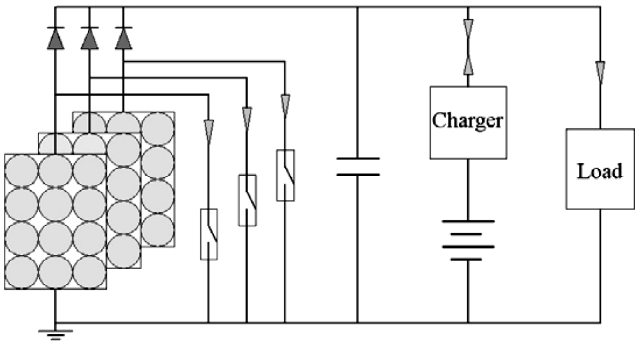

Fig. 4 Sequential shunt-switching regulation.

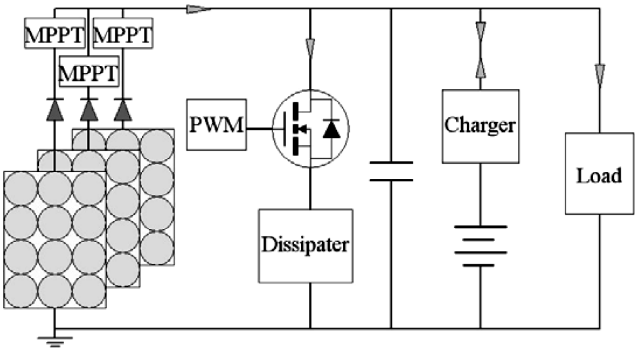

Fig. 5 Proposed PWM-controlled shunt regulation with MPP tracking.

In the system in Fig. 3, sequential series switches[11] are used. Each individual solar array panel is connected to the main power bus through a switch that is operated in on or off state and controlled according to the bus voltage level setpoint. The disadvantages of this configuration are as follows. First, the impedance across the rail seen by the solar arrays during a switch on state is determined by the battery state of charge and the load conditions, which generally cannot satisfy the maximum power transfer condition. Second, all of the absorbed solar power will be dissipated in the solar arrays as heat during the switch off state, which induces thermal stress and, due to the thermal inertia of the array, causes efficiency degradation at the time when the switch is back in the on state. Third, on- and off-state operations of series switches give rise to a jagged bus voltage; therefore a large filter capacitance or an active filtering device is required to keep the voltage ripple at an acceptable level.

The system shown in Fig. 4 uses a sequential shunt-switching configuration.[12] Disadvantages similar to those of sequential series-switching, such as large voltage ripples and nonmaximized power transfer, exist in this system, likewise, due to the binary nature of the switch operation. The advantage of the sequential shunt-switching over the sequential series-switching is that a small portion of the excess energy is shunted to the panel structural frame (serving as an electrical ground) during the switch on state. However, the majority of heat still dissipates in the cell because the shunt does not provide the array with any maximum power and heat transfer mechanism. Thus, the comparatively lower power capability of the solar arrays of both sequential series and shunt regulations and their requirements for large filters result in unnecessarily great mass and volume in the overall system design.

To address these problems, we propose the system shown in Fig. 5. In this configuration, the power generated by each panel of solar arrays feeds the bus through an MPP tracker.[13,14] Across the bus rail, one or more PWM-controlled shunts for example, power metal-oxide-semi conductor field-effect transistor switches (only one shown in Fig. 5), are connected. The shunts act as bypasses for the excess power and facilitate the solar array with varying impedance for the maximum power transfer. The excess power is dissipated as heat in the dissipater that also serves as a radiator transporting the heat into space. For the most effective heat dissipation, the dissipater can be placed on the back of the array panel, where the sun-viewing factor is zero, and the Earth albedo, the Earthshine and the satellite heat radiation viewing factors are minimized, while the space-view factor is maximized. The detailed design of the dissipater, including geometry, mass, and thermal efficiency, are beyond the scope of this paper; the means to transfer efficiently the heat to space without adding significant size and mass penalty will be a focus in the next stage of our research.

The advantages of the system shown in Fig. 5 can be summarized as follows. 1) The solar array is always operated at its MPP; therefore, the highest efficiency can always be achieved. When it is considered that the added weight and volume of the controllers are minimal (compared to sequential switching regulations that also use electronic controllers and switches), it is clear that the size and mass of the solar array for a given power requirement is lower than is the case with the sequential series- or shunt-switching regulations. 2) Given the same thermal environmental conditions, the solar array in this system undergoes minimized self-dissipation because of maximum power delivery to the bus. This results in the lowest possible cell temperature, preferable to that resulting from the sequential series- or shunt-switching regulations. The direct benefits are less reversible thermal degradation and better voltage regulation. 3) Under the condition of a partial failure of cells in an array due to sporadic damage from impact of microextraterrestrial objects or due to other reasons such as mechanical stress during deployment, etc., it is especially beneficial to use the MPP because the best efficiency and the lowest temperature of the array are still obtained. Otherwise, the altered array internal resistance will result in impedance mismatching and considerable power loss.[3] 4) The characteristics of the PWM-controlled shunt allow high-quality bus voltage regulation with minimized ripples because the shunt provides continuously varying impedance across the rail and bypasses any level of excess power. Therefore, the filter can be minimized. These advantages will be evident in the process of our analysis in the next section.

Efficiency Analysis

In this section, we present a preliminary analysis of the efficiency and operating temperature of the solar array for the proposed system based on a simplified model. The temperature of the solar arrays is governed by the following dynamic equation:

$$c_p m \frac{\mathrm{d}T}{\mathrm{d}t} = q_{\mathrm{SS}} + q_{\mathrm{EA}} + q_{\mathrm{ES}} + q_{\mathrm{SP}} + q_{\mathrm{SA}} + q_{\mathrm{ST}} \qquad (1)$$

where the left-hand side of the equation is the rate of change of the array internal energy that depends on the array temperature T and the right-hand side is the rate of heat input in watts. Each of the heat rate components, those from sunshine q_{SS}, Earth albedo q_{EA}, Earthshine q_{ES}, space heat sink q_{SP}, solar array radiation cooling q_{SA}, and satellite internal heat generation q_{ST}, is explained in the Appendix.

For a circular LEO with an altitude of 798 km, the orbital period is about 100.73 min. It is assumed that the satellite has a sun-view time of 70% of its orbital period and an Earth-shadow time of 30%.

Table 2 Cell parameters

Cell	m_a, kg/m^2	c_p, J/kg · K[a]	α	ε	γ	η_{mp} % 301K	320 K	350 K
$GaInP_2$/GaAs/Ge (ITJ)[b]	2.06	460	0.92	0.85	0.84	26.8	25.6	23.7
Si K4702 (SJ)[b]	1.07	700	0.74	0.85	0.74	13.3	12.3	10.7
CIGS (TF)[c]	0.7	330	0.92	0.85	0.94	15	13.4	11

[a]Estimated nominal value. [b]Spectrolab website. [c]Data for α, ε, and γ are assumed values.

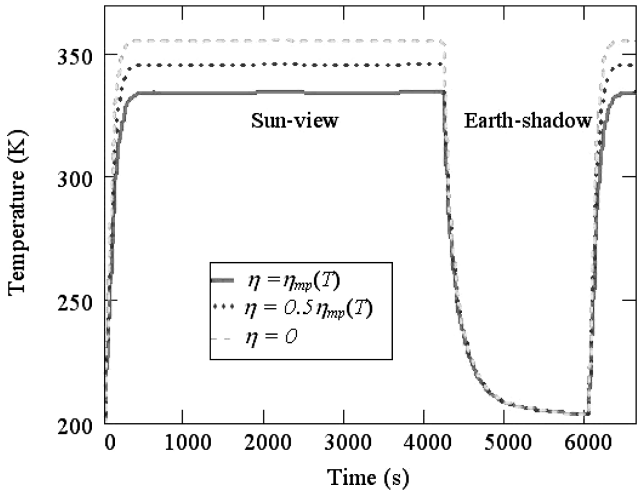

Fig. 6 Temperatures of the $GaInP_2$/GaAs/Ge ITJ cell at three operation modes; sun-view time values of 334.9, 346.2, and 355.9 K.

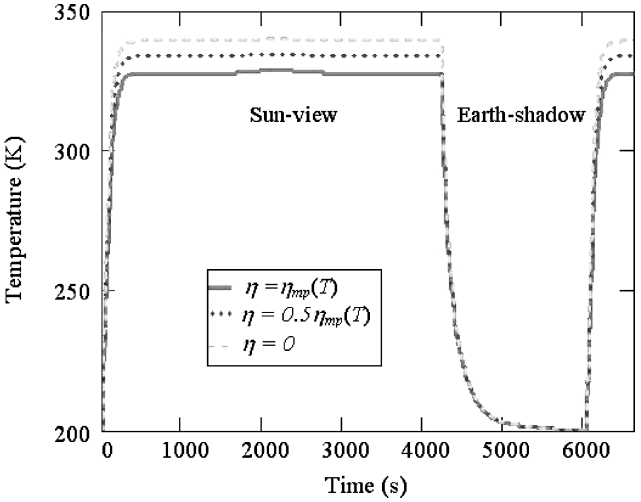

Fig. 7 Temperatures of Si K4702 SJ cell at three different modes; sun-view time values of 328.9, 334.8, and 340.1 K.

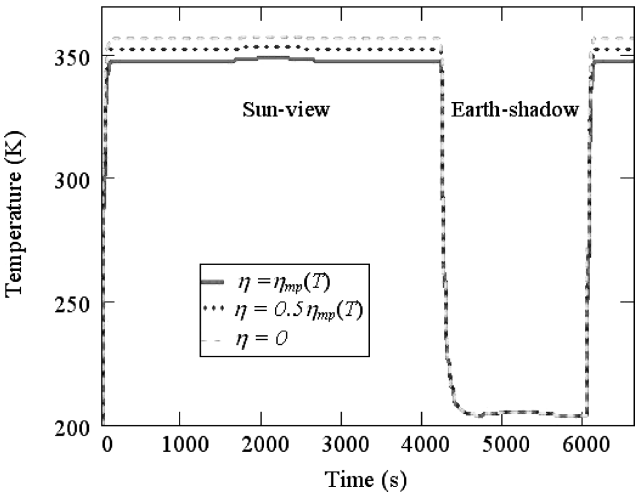

Fig. 8 Temperatures of the CIGS TF cell at three different modes; sun-view time values of 348.9, 353.6, and 357.8 K.

Also, we assume that the solar array is at the beginning of its life, and the day of the orbiting is 8 April 2003. Therefore, the solar constant is 1366.1 W/m^2. Table 2 lists parameters for three types of solar cells that are studied in the proposed system for comparison: the $GaInP_2$/GaAs/Ge improved triple-junction cell (ITJ), the Si single-junction cell (K4702), and the CIGS thin-film cell. The solar absorptance and the thermal emittance for the first two cells are from the Spectrolab products website given earlier. The absorptance and the emittance for the CIGS are assumed values because the data are not available. Also notice that, although both the solar absorptance and the thermal emittance of a cell are applicable to certain spectral regions only, the detailed characteristics of the absorptivity and emissivity for each cell are ignored in Eq. (1) for simplicity. This assumption does not introduce significant errors into the analysis.

The mechanical and electrical characteristics of the three cells are different. The CIGS thin film has the least specific mass, whereas the Si K4702 has the lowest solar absorptance and efficiency. The GaAs-based ITJ cell is the highest in efficiency and also has the highest specific mass. The specific mass listed here accounts for both the cells and the structure. Table 2 also lists the maximum efficiencies of the cells for temperatures of 301, 320, and 350 K. Operation of these three types of cells is conducted in three modes: 1) The cells are always operated at their maximum efficiencies, which corresponds to the case of using the proposed system. 2) The cells are operated at 50% of their maximum efficiencies. 3) The cells are operated at 0% efficiency, which corresponds to the case that all of the absorbed solar power is dissipated in the cells as heat. Whereas no solar arrays are constantly operated at 50 or 0% efficiencies, these calculations are performed for purposes of comparison.

Figures 6–8 show the temperature variations of the solar arrays for the $GaInP_2$/GaAs/Ge ITJ cell, the Si K4702 SJ cell, and the CIGS TF cell, respectively, for the time duration of about 1.1 orbits (total 110.8 min or 6648 s). For each cell, three temperature curves are generated, which correspond to the maximum power transfer (solid curves), 50% of maximum power transfer (dotted curves), and zero power transfer (dashed curves). As can be seen, during the Earth shadow time, the temperature of cells does not drop to the space background temperature due to the thermal environment of satellite internal heat generation and Earthshine at a near Earth orbit. During the sun illumination time, the temperature is lowest when the array is operated at the MPP, being 334.9, 328.9, and 348.9 K, respectively, for the three cells. Consequently, the thermally induced efficiency losses are 8, 11.3, and 26.7%. If, however, the solar arrays are operated at 50% of the MPP, the temperatures increase to 346.2, 334.8, and 353.6 K at the sun-view time, and the corresponding thermally induced losses increase to 10.8, 13.5, and 28.7%. The total losses, including both the thermally induced loss and that due to impedance mismatching, are 55.4, 56.8, and 64.3%. Of course, in an extreme case such as when the arrays are open circuited or the impedances are severely mismatched, no power (or only little power) will be transferred to the bus, and the temperatures for the three cells will increase to 355.9, 340.1, and 357.8 K, respectively, yielding thermally induced losses of 13.1, 15.8, and 31.3%.

Table 3 Cell performance

Operation	Cell		
	$GaInP_2$/GaAs/Ge (ITJ)	Si K4702 (SJ)	CIGS (TF)
MPP			
T, K	334.9	328.9	348.9
T-induced loss, %	8	11.3	26.7
Total loss, %	8	11.3	26.7
50% MPP			
T, K	346.2	334.8	353.6
T-induced loss, %	10.8	13.5	28.7
Total loss, %	55.4	56.8	64.3
0 Power			
T, K	355.9	340.1	357.8
T-induced loss, %	13.1	15.8	31.3
Total loss, %	100	100	100

Table 4 Coefficient for equivalent sunshine

Cell	κ_{EA}	κ_{ES}	κ_{ST}
$GaInP_2$/GaAs/Ge (ITJ) at 320 K	0.103	0.049	0.070
Si K4702 (SJ) at 340 K	0.084	0.040	0.070
CIGS (TF) at 350 K	0.103	0.049	0.070

The results shown in Figs. 6–8 are summarized in Table 3. In Table 3, the thermally induced efficiency losses are listed for three operation modes for the three types of cells. In addition, the total efficiency losses are also listed. Without MPP tracking, significant loss results due to impedance mismatching, which causes the cell temperature to rise even higher and further increases thermal loss. With the MPP tracking, the loss due to impedance mismatching is eliminated, resulting in the lowest temperature and minimized thermal degradation. Notice that in each operation mode analyzed, the temperature of the Si cell is the lowest among the three. This is a result of the relatively low solar absorptance of that cell (74%). Therefore, an appropriate coating that transmits the photovoltaic spectrum while blocking heat irradiation can significantly reduce the cell operating temperature and improve the power output.

The systems without MPP tracking can be operated at a power point determined by the battery state of charge and the load impedance, which typically varies in time. In this case, because the amount of power transferred to the bus depends on instantaneous impedance matching conditions, the power dissipation in the cell changes accordingly. This results in oscillations of the cell temperature between the values corresponding to a maximum power transfer and those corresponding to a zero power transfer. Once the temperature is maximized, even if the impedance is matched at some instant during operation, the power transfer is still severely limited due to an already degraded efficiency, causing considerable energy and power loss. To illustrate this limitation, we calculate the time required for the array temperature to change from the highest to the lowest during an MPP operation. When the heat input due to the space heat sink is ignored, the array temperature at any time t during a sun-view period can be approximately calculated according to

$$c_p m \frac{\mathrm{d}T}{\mathrm{d}t} \approx -2A\sigma\varepsilon T^4 + [1 - \rho - \eta(T) + \kappa_{EA} + \kappa_{ES} + \kappa_{ST}]AS \quad (2)$$

Equation (2) is a simplified version of Eq. (1), where the heat transfers due to Earth albedo, Earthshine, and satellite internal heat are converted to the equivalent amount of sunshine using the parameters κ_{EA}, κ_{ES}, and κ_{ST}, which can be evaluated for their averaged values using Eqs. (A4), (A5), and (A8). A solution to Eq. (2), the time for the array temperature changing from the maximum to the minimum, is given by Eq. (A10). When the material properties for the three types of cells listed in Table 2, and the parameters for equivalent sunshine listed in Table 4 are used, the temperature swing time is 376 s for the $GaInP_2$/GaAs/Ge ITJ cell, 223 s for the Si K4702 SJ cell, and 30 s for the CIGS TF cell. The conclusion is that it takes at least 6 min for the $GaInP_2$/GaAs/Ge ITJ cell to reduce its temperature to the optimized value once the temperature is elevated, during which time the power transfer is severely limited. For the CIGS thin-film cell, the swing time reduces to a half-minute due to its light weight and low specific heat. Notice that the swing time was calculated using the MPP tracking condition. Without MPP, it will take a longer time, or it may never reach the minimum temperature. Apparently, constant MPP tracking not only maximizes the power output, but also improves the system capability for dynamic voltage regulation.

Design Application

In general, the load of the satellite power system is mission dependent and varies during the course of orbiting. For simplicity, we assume that a constant load is applied to the system during the entire satellite service life. In this case, the battery has to supply the total power to the load during the Earth-shadow time. An energy balance equation for the system can be written as follows:

$$D\Gamma \cdot P_{SA} = \Gamma \cdot P_L \quad (3)$$

When the solar array efficiency is used, the desired solar array power can be expressed as

$$P_{SA} = P_L/D = \delta\gamma\eta_{mp}(T)AS_0 \quad (4)$$

where δ is the power transfer factor, $\delta = 1.0$ for a maximum power delivery, and γ is the efficiency degradation factor due to radiation, which is the primary factor affecting the service lifetime of solar cells. The efficiency value η in Eq. (4) represents reversible efficiency degradation mechanisms as a function of temperature and does not include the permanent degradation due to thermal stress, which is generally not a concern.[3] Sporadic array damage due to the impact of microextraterrestrial objects is not considered in Eq. (4). Hence, the size and the mass of the solar array based on the condition at the end of life (EOL) can be designed according to

$$A(T, \delta, \gamma) = \frac{P_L}{\delta\gamma\eta_{mp}(T)DS_0} \quad (5)$$

$$m(T, \delta, \gamma) = \frac{m_a P_L}{\delta\gamma\eta_{mp}(T)DS_0} \quad (6)$$

where m_a is the specific mass of solar arrays. Here, the area and the mass of the solar array are written as explicit functions of the temperature, the power transfer factor, and the radiation degradation factor because these three parameters significantly affect the cell performance. For a particular mission, the parameters P_L, D, and S_0 are given. Equations (5) and (6) can be normalized as

$$A_n(T, \delta, \gamma) = 1/\delta\gamma\eta_{mp}(T) \quad (7)$$

$$m_n(T, \delta, \gamma) = m_a/\delta\gamma\eta_{mp}(T) \quad (8)$$

The normalized area is a number that specifies the cell power generation capability in terms of area compared to the unit area of a cell for a given load power, solar irradiance, and sun-view duty ratio in an orbit. The lower the number of the normalized area, the better the power capability will be. Similarly, the normalized mass number specifies the cell power generation capability in terms of mass. In the calculations, the radiation degradation factors (listed in Table 2) for the $GaInP_2$/GaAs/Ge ITJ cell, the Si K4702 SJ cell, and the CIGS TF are 0.84, 0.74, and 0.94, respectively, at the EOL.

For the first two cells, the data were obtained under an irradiation fluence of 1×10^{15} electrons/cm^2 at 1 MeV (Spectrolab products website), which is approximately equivalent to the radiation received by an Si cell at the LEO environment during a period of 10 years.[15] Thin-film cells are considered to have the best radiation hardness. Previous experimental results[16] show about 10% improvement in terms of radiation degradation tolerance for the CIGS cell compared to that of the GaAs-based triple-junction cell. Also, in Eqs. (7) and (8), the cells are assumed to be operating under the maximum power transfer conditions.

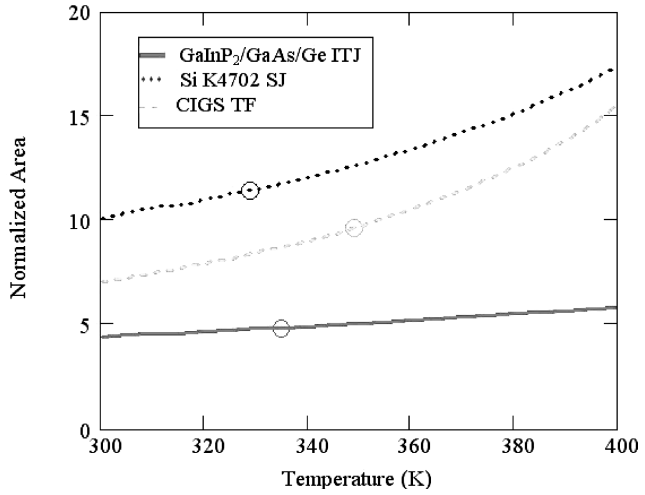

Fig. 9 Normalized area number as a function of temperature for three types of cells.

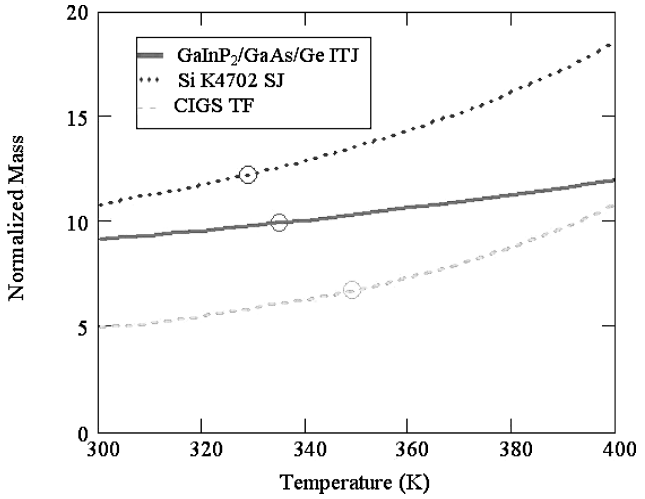

Fig. 10 Normalized mass number as a function of temperature for three types of cells.

Figures 9 and 10, respectively, show the area number and the mass number as a function of temperature for three types of cells using the described degradation factors and operation conditions. The area and mass numbers marked by the circles in Figs. 9 and 10 correspond to the thermal conditions obtained from Figs. 6–8 for three types of cells. Figure 9 shows that the $GaInP_2/GaAs/Ge$ ITJ cell has the lowest area number in the 300–400 K temperature range because of its highest efficiency. In contrast, the other two cells have higher area numbers, with the CIGS performing better than the Si cell. For the maximum power transfer under given thermal conditions, the area numbers are 4.83 for the $GaInP_2/GaAs/Ge$ ITJ cell, 11.46 for the Si K4702 SJ cell, and 9.63 for the CIGS TF cell.

In practical design, the solar array mass is the most important parameter because the cost for satellite launching and maneuvering in orbit is directly related to the total mass. The comparison of the mass numbers for three types of cells is given in Fig. 10. For the given thermal environment with a maximum power delivery, they are 9.94 for the $GaInP_2/GaAs/Ge$ ITJ cell, 12.27 for the Si cell, and 6.74 for the CIGS cell. Clearly the CIGS cell outperforms the other two cells with respect to the mass numbers.

Although the CIGS cell has the lowest mass number, it bears the largest area number among three cells. However, greater area yields disadvantages in deployability, maintenance, and reliability. An optimal design should consider both mass and area to achieve maximum system efficiency, power density, life and reliability, while minimizing the risk of damage and cost. In the following discussion, we consider design optimization for a simplified case by including

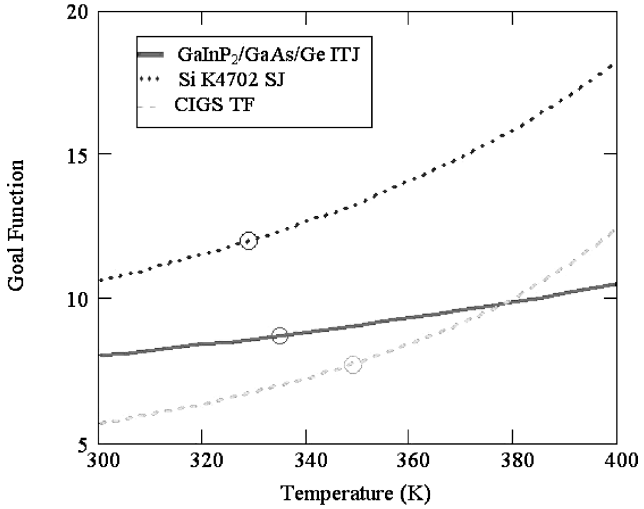

Fig. 11 Goal function numbers of the three types of cells with maximum power transfer.

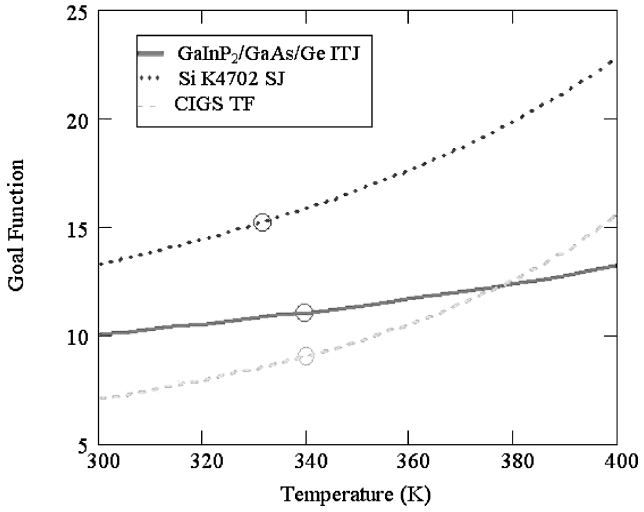

Fig. 12 Goal function numbers of the three types of cells with 80% maximum power transfer.

both mass and area numbers, together with a maximum power delivery under a given thermal environment. An optimization goal function may be chosen as

$$G(T, \delta, \gamma) = \sqrt{\xi \cdot A_n(T, \delta, \gamma)^2 + \zeta \cdot m_n(T, \delta, \lambda)^2} \qquad (9)$$

Here ξ and ζ are weight factors for the area and mass numbers, respectively. The weight coefficients largely depend on practical design considerations and have been chosen here for demonstration purposes as $\xi = 0.3$, and $\zeta = 0.7$. Figure 11 shows the goal function as a function of temperature for the three cells. Below 380 K, the CIGS cell has the best performance, whereas above 380 K the $GaInP_2/GaAs/Ge$ ITJ cell performs the best. Under the optimized power transfer and given thermal conditions, the numbers yielded from the goal function are 8.73 for the $GaInP_2/GaAs/Ge$ ITJ cell, 12.03 for the Si cell, and 7.72 for the CIGS cell, which, therefore, shows the best performance.

For comparison, Fig. 12 shows the goal function numbers for three types of cells with 80% maximum power transfer. In this case, the temperatures of the cells are elevated, and the corresponding mass and area have to be increased. The numbers of the goal function for the three cells are 11.05 for the $GaInP_2/GaAs/Ge$ ITJ cell, 15.21 for the Si cell, and 9.03 for the CIGS cell. Again the result is that the CIGS has the best performance due to its light weight and good radiation tolerance. However, the CIGS is still in development, and its applicability for space applications remains to be proven. Thus, among the state-of-the-art cells, the GasAs-based ITJ cell is a better

choice than the Si cell because its performance is very similar to that of the CIGS.

Note that under the condition of the maximum power operation, the power delivered to the bus is less than the maximum power generated by the solar array because part of the power is bypassed to the dissipater through the shunt. Therefore, in the design Eqs. (7–9), the power transfer factor δ is always less than 1. In this analysis, we simplified the consideration of δ to illustrate the benefits of the maximum power operation. In practical design, the value for δ must be carefully determined based on the particular system design and satellite mission specifications.

Conclusions

A design for MPP tracking and PWM-controlled shunt regulation for satellite power systems has been proposed to minimize thermal degradation and maximize efficiency. A preliminary analysis of the performance of three typical cells, based on a simplified thermal dynamic model of a solar array in orbit, is presented for the cases of MPP operations and non-MPP operations. The analysis shows that the proposed design offers the advantages of maximum power delivery, highest cell efficiency, lowest cell temperature, and minimized bus voltage ripples compared to the existing bus regulation methods. Therefore, it allows better quality of bus voltage regulation, as well as smaller size and longer service lifetime of solar arrays.

Appendix: Heat Transfer Rates

Solar Irradiance in a Circular Orbit

A circular orbit is a good approximation for the low Earth satellite orbit. The time for one orbit can be calculated as

$$\Gamma = \left(2\pi \Big/ \sqrt{\mu}\right)(R_{\mathrm{EA}} + H_{\mathrm{ST}})^{\frac{3}{2}} \tag{A1}$$

The solar irradiance varies for orbital positions. For a circular orbit of approximately 1 astronomical unit from the sun, it can be assumed as a constant for the portion of the orbit that is exposed to the sun's illumination and zero for the portion in the Earth's shadow. Therefore,

$$S(t) = S_0 \sum_{k=1}^{N} [\Phi(t - (k-1)\cdot\Gamma) - \Phi(t - (k-1+D)\cdot\Gamma)] \tag{A2}$$

Heat Transfer due to Sunshine

Assume that sunrays are always perpendicular to the surface of the solar arrays. The percentage of the solar power that turns to heat is $\lfloor 1 - \rho_{f,\mathrm{SA}} - \eta(t) \rfloor$. The heat transfer rate due to sunshine can be described as

$$q_{\mathrm{SS}}(t) = \lfloor 1 - \rho_{f,\mathrm{SA}} - \eta(t) \rfloor A S(t) \tag{A3}$$

Notice that the heat in Eq. (A3) includes both direct heat from the sun and the array internal ohmic heat.

Heat Transfer due to Earth Albedo

The Earth albedo is about 0.35. The atmospheric transmittance is about 0.74. Both the front and back surfaces of the solar array absorb the heat resulting from the Earth albedo. The heat transfer also depends on the satellite altitude, the array surface absorptance, and the array Earth-viewing factor. These phenomena can be described by the following equation:

$$q_{\mathrm{EA}}(t) = [R_{\mathrm{EA}}/(R_{\mathrm{EA}} + H_{\mathrm{ST}})]^2 \times [\alpha_{f,\mathrm{SA}}\beta_{f,\mathrm{EA}}(t) + \alpha_{b,\mathrm{SA}}\beta_{b,\mathrm{EA}}(t)] A \tau_{\mathrm{AT}} \rho_{\mathrm{EA}} S(t) \tag{A4}$$

Heat Transfer due to Earthshine

Similarly, the heat transfer rate due to the Earthshine is given by

$$q_{\mathrm{ES}}(t) = [R_{\mathrm{EA}}/(R_{\mathrm{EA}} + H_{\mathrm{ST}})]^2 \times [\alpha_{f,\mathrm{SA}}\beta_{f,\mathrm{EA}}(t) + \alpha_{b,\mathrm{SA}}\beta_{b,\mathrm{EA}}(t)] A \tau_{\mathrm{AT}} \sigma \varepsilon_{\mathrm{EA}} T_{\mathrm{EA}}^4 \tag{A5}$$

where we assume that the Earth is in thermal equilibrium state[17] and the temperature is $T_{\mathrm{EA}} = 270$ K. A more sophisticated model can be developed based on the consideration of temperature distributions on the surface of the Earth depending on the time, day, and session. For our preliminary analysis, we use the simplified relation (A5).

Heat Transfer due to Space Heat Sink

Space heat transfer rate depends on the solar array surface absorptance, space-viewing factor, and space background temperature. The heat transfer rate can be calculated as

$$q_{\mathrm{SP}}(t) = [\alpha_{f,\mathrm{SA}}\beta_{f,\mathrm{SP}}(t) + \alpha_{b,\mathrm{SA}}\beta_{b,\mathrm{SP}}(t)] A \sigma \varepsilon_{\mathrm{SP}} T_{\mathrm{SP}}^4 \tag{A6}$$

Radiation Cooling

The amount of heat emitted into the space environment by solar arrays can be computed as

$$q_{\mathrm{SA}}(t) = -\sigma[\varepsilon_{f,\mathrm{SA}} + \varepsilon_{b,\mathrm{SA}}] A T^4 \tag{A7}$$

Heat Transfer due to Onboard Heat Sources

The heat transfer rate due to onboard heat sources depends on the solar array surface absorptance, the satellite-viewing factor, and the satellite temperature:

$$q_{\mathrm{ST}}(t) = [\alpha_{f,\mathrm{SA}}\beta_{f,\mathrm{ST}}(t) + \alpha_{b,\mathrm{SA}}\beta_{b,\mathrm{ST}}(t)] A \sigma \varepsilon_{\mathrm{ST}} T_{\mathrm{ST}}^4(t) \tag{A8}$$

In Eq. (8), an equilibrium temperature for the satellite is assumed. This temperature is generally a function of time. For a given satellite and its operation, the exact heat rate may be calculated as

$$\sigma \varepsilon_{\mathrm{ST}} T_{\mathrm{ST}}^4(t) = \dot{q}_{\mathrm{ST}}(t) \tag{A9}$$

Approximations

Some approximations made in the preceding equations are commented on here. 1) The solar irradiance in orbit fluctuates due to the sun's surface activities and the Earth's elliptical orbit and inclination. These effects are ignored for simplicity. 2) Each panel of the solar arrays is assumed to have an equal area for its front and back surfaces. The photovoltaic effect active area is assumed to be equal to that of the front surface as well. 3) The temperature of the Earth's surface is a function of location, time, day, and session. A thermal equilibrium state is assumed for simplicity. 4) The heat transfer due to satellite onboard sources is a function of time, depending on a particular satellite design and mission. Again for simplicity, a constant value is assumed. 5) The solar array Earth-viewing factor, space-viewing factor, and satellite-viewing factor are complicated functions of the solar array and satellite geometries, position, orientation, and orbital parameters. It is assumed that the solar array has a fixed orientation with respect to the satellite, and it always faces the sun. Therefore, the satellite viewing-factor is a constant. The Earth- and space-viewing factors are functions of time and orbital positions.

Estimation of Array Temperature Swing Time

When an averaged maximum efficiency is assumed, a solution to Eq. (2), the time for the array temperature to change from the maximum value to the minimum value is

$$\vartheta = -\frac{k}{4b}\,\ell_n\left[\frac{(k - T_{\min})(k + T_{\max})}{(k + T_{\min})(k - T_{\max})}\right] + \frac{k}{2b}\left[a\tan\left(\frac{T_{\min}}{k}\right) - a\tan\left(\frac{T_{\max}}{k}\right)\right] \tag{A10}$$

$$b = \frac{1 - \rho - \eta_{\mathrm{mp}} + \kappa_{\mathrm{EA}} + \kappa_{\mathrm{ES}} + \kappa_{\mathrm{ST}}}{c_p m_a} S_0 \tag{A11}$$

$$k = \left(\frac{1 - \rho - \eta_{\mathrm{mp}} + \kappa_{\mathrm{EA}} + \kappa_{\mathrm{ES}} + \kappa_{\mathrm{ST}}}{2\sigma\varepsilon} S_0\right)^{\frac{1}{4}} \tag{A12}$$

where $m_a = m/A$ is the array specific mass.

Acknowledgments

This work is partially supported by National Reconnaissance Office (NRO) under Grant 00-C-1034 and by the Office of Naval Research under Grant N00014-00-1-0368.

References

[1]Wysocki, J. J., and Rappaport, P., "Effect of Temperature on Photovoltaic Solar Energy Conversion," *Journal of Applied Physics*, Vol. 31, March 1960, pp. 571–578.

[2]Scheiman, D. A., Jenkins, P. P., Brinker, D. J., and Appelbaum, J., "Low Intensity Low Temperature (LILT) Measurements and Coefficients on New Photovoltaic Structures," *Progress in Photovoltaics: Research and Applications*, Vol. 4, No. 2, 1996, pp. 117–127.

[3]Hoffman, D. J., and Scheiman, D. A., "Thermal Cycling of Mir Cooperative Solar Array (MCSA) Test Panels," NASA TM-107511, July–Aug. 1997.

[4]Hegedus, S., McCandless, B. E., and Birkmire, R., "Analysis of Stress-Induced Degradation in CdS/CdTe Solar Cells," *28th IEEE Photovoltaic Specialists Conference Record*, IEEE Press, Piscataway, NJ, 2000, pp. 535–538.

[5]"SOLAR2000 Total Irradiance File," U.S. Dept. of Commerce, NOAA, Space Environment and Space Environment Technologies, URL: http://www.sel.noaa.gov/ftpmenu/lists/spacewx.html. [cited 20 April 2003].

[6]Tobiska, W. K., Woods, T., Eparvier, F., Viereck, R., Floyd, L., Bouwer, D., Rottman, G., and White, O. R., "The SOLAR2000 Empirical Solar Irradiance Model and Forecast Tool," *Journal of Atmospheric and Solar–Terrestrial Physics*, Vol. 62, No. 14, 2000, pp. 1233–1250.

[7]Tobiska, W. K., and Nusinov, A. A., "Status of the Draft ISO Solar Irradiance Standard," *Physics and Chemistry of Earth* Part C: Terrestrial and Planetary Science, Vol. 25, No. 5–6, 2000, pp. 387–388.

[8]Colozza, A., "Convective Array Cooling for a Solar Powered Aircraft," NASA/CR-2003-212084, Jan. 2003.

[9]Hoffman, D., "A Parametric Assessment of the Mission Applicability of Thin-Film Solar Arrays," NASA TM-2002-211720, Aug. 2002.

[10]Clark, C., Wood, J., and Zuckermandel, B., "Self-Deploying, Thin-Film PV Solar Array Structure," *2002 Core Technologies for Space Systems Conference*, URL: http://www.spacecoretech.org/coretech2002/Papers [cited 10 Nov. 2003].

[11]Weinberg, A., "Solar Array System," U.S. Patent, US6262558 B1, 17 July 2001.

[12]Barry, R. K., "Conversion from Full Array Shunt to Partial Shunt Topology for Two Small Explorer-Class, Near-Earth Orbiting Scientific Satellites," *Proceedings of the 31st Intersociety Energy Conversion Engineering Conference*, Vol. 1, IEEE Press, Piscataway, NJ, 1996, pp. 525–528.

[13]Enslin, J. H. R., "Maximum Power Point Tracking: A Cost Saving Necessity in Solar Energy Systems," *IECON'90, 16th IEEE IES Annual Conference*, Vol. 2, IEEE Press, Piscataway, NJ, 1990, pp. 1073–1077.

[14]Beukes, H. J., and Enslin, J. H. R., "Analysis of a New Compound Converter as MPPT, Battery Regulator and Bus Regulator for Satellite Power Systems," *PESC'93 Record, 24th Annual IEEE PESC*, IEEE Press, Piscataway, NJ, 1993, pp. 846–852.

[15]Gregor, I. M., and Weidberg, T., "Results of the Fluence Calculations for the Pixel Detector," URL: http://www-pnp.physics.ox.ac.uk/~weidberg/fluences.html [cited 21 Nov. 2003].

[16]Bätzner, D. L., Romeo, A., Tiwari, A. N., and Zogg, H., "Stability of CdTe Solar Cells for Terrestrial and Space Applications," Thin Film Physics, Annual Report URL: http://www.tfp.ethz.ch/ [cited 21 Nov. 2003].

[17]Juhasz, A. J., "An Analysis and Procedure for Determining Space Environmental Sink Temperatures with Selected Computational Results," NASA TM-2001-210063, Jan. 2001.